CHEMISTRY OF MATERIALS

pubs.acs.org/cm

Article

Diamagnetic d-Orbitals Drive Magnetic Structure Selection in the Double Perovskite Ba_2MnTeO_6

Otto H. J. Mustonen, Charlotte E. Pughe, Helen C. Walker, Heather M. Mutch, Gavin B. G. Stenning, Fiona C. Coomer, and Edmund J. Cussen*

Cite This: *Chem. Mater.* 2020, 32, 7070−7079

Read Online

ACCESS | Metrics & More | Article Recommendations | Supporting Information

ABSTRACT: B-site ordered $A_2B'B''O_6$ double perovskites have a variety of applications as magnetic materials. Here, we show that diamagnetic d^{10} and d^0 B″ cations have a significant effect on the magnetic interactions in these materials. We present a neutron scattering and theoretical study of the Mn^{2+} double perovskite Ba_2MnTeO_6 with a $4d^{10}$ Te^{6+} cation on the B″-site. It is found to be a Type I antiferromagnet with a dominant nearest-neighbor J_1 interaction. In contrast, the $5d^0$ W^{6+} analogue Ba_2MnWO_6 is a Type II antiferromagnet with a significant next-nearest-neighbor J_2 interaction. This is due to a d^{10}/d^0 effect, where the different orbital hybridization with oxygen 2p results in different superexchange pathways. We show that d^{10} B″ cations promote nearest neighbor and d^0 cations promote next-nearest-neighbor interactions. The d^{10}/d^0 effect could be used to tune magnetic interactions in double perovskites.

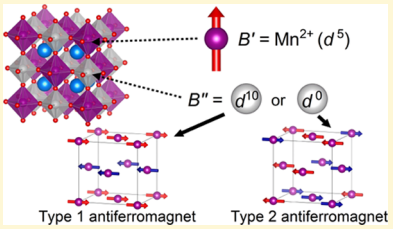

1. INTRODUCTION

The B-site ordered $A_2B'B''O_6$ double perovskite family of oxides has been widely investigated for their varied functional properties. In terms of magnetic materials, double perovskites have potential applications as ferro- and ferrimagnets with high Curie temperatures, as half-metallic ferromagnets in spintronics and as multiferroic materials.[1] The magnetic ground state and transition temperature of a material are determined by the interactions between its magnetic cations. In oxides, the main interactions are usually superexchange interactions mediated by oxygen 2p orbitals. The semiempirical Goodenough−Kanamori rules[2−4] predict superexchange interactions in materials, where two transition metal cations are separated by an oxygen anion in either a 90° or a 180° bond angle.

The situation is more complicated in compounds where the magnetic cations are further apart. This occurs in double perovskites with one magnetic and one diamagnetic B-site cation alternating over the sites of the structure giving rock-salt order. Diamagnetic d^{10} and d^0 cations can act as linkers between magnetic cations in extended superexchange pathways and can lead to very different magnetic interactions. This is due to an orbital hybridization mechanism, where the empty d^0 orbitals can readily hybridize with O 2p orbitals whereas the full d^{10} states tend to be significantly below the Fermi level.[5] This d^{10}/d^0 effect has been firmly established in B-site ordered Cu^{2+} double perovskites $Sr_2Cu(Te,W)O_6$ and $Ba_2Cu(Te,W)O_6$, where Te^{6+} is a $4d^{10}$ cation and W^{6+} is a $5d^0$ cation on the B″-site linking the CuO_6 octahedra.[6−13] Despite being isostructural, interactions in the Te^{6+} and the W^{6+} compounds are completely different: both Sr_2CuTeO_6 and Ba_2CuTeO_6 have dominant nearest-neighbor J_1 interactions, whereas Sr_2CuWO_6 and Ba_2CuWO_6 have dominant next-nearest-neighbor J_2 interactions.[8,10] Furthermore, a novel spin-liquid-like state has been reported for the solid solution $Sr_2CuTe_{1-x}W_xO_6$.[13−16]

These Cu^{2+} compounds are not representative of double perovskites in general for a number of reasons. The Cu^{2+} double perovskites are tetragonally distorted by the Jahn−Teller activity of this cation resulting in more complicated interactions. Octahedral tilts are closely linked to the overall strength of magnetic interactions in these materials.[17] Most importantly, due to orbital ordering of the $3d^9$ Cu^{2+} cations, the magnetism in these materials is highly two-dimensional unlike in other double perovskites.[8,10,17] The interactions only involve the unoccupied $3d_{x^2-y^2}$ orbitals of the copper cations. Finally, quantum effects such as quantum fluctuations are significant because of the $S = 1/2$ nature of the Cu^{2+} cation. Therefore, it remains an open question of whether the d^{10}/d^0 effect is specific to these Cu^{2+} compounds or whether it is more widely applicable.

The change in the dominant magnetic interaction observed in the copper double perovskites does not occur in $4d^3$ Ru^{5+} and $5d^3$ Os^{5+} double perovskites, which all have a dominant J_1 interaction.[18−21] A theoretical study of magnetic interactions in the monoclinic Os^{5+} double perovskites Sr_2InOsO_6 (d^{10}) and Sr_2ScOsO_6 and Sr_2YOsO_6 (d^0) found a strong connection between the B″ cation and overall strength of magnetic interactions.[21] While these compounds all have the same Type I antiferromagnetic structure, magnetic interactions are the

Received: July 17, 2020
Revised: July 23, 2020
Published: July 23, 2020

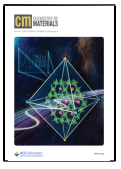

https://dx.doi.org/10.1021/acs.chemmater.0c02971
Chem. Mater. 2020, 32, 7070−7079

strongest in Sr_2ScOsO_6 due to significant hybridization of Sc $3d^0$ states with O 2p and Os 5d states. Interactions in the d^{10} Sr_2InOsO_6 were found to be the weakest, as the hybridization of the filled In $4d^{10}$ states with O 2p states were found to be very weak.[21] Differences between materials with d^{10} or d^0 linking cations have also been reported for $5d^2$ Os^{6+} compounds.[22] In general, interpretation of the d^{10}/d^0 effect in these 4d and 5d double perovskites is complicated by the strong spin−orbit coupling of the magnetic cations.[18]

The Mn^{2+} double perovskites Ba_2MnTeO_6 and Ba_2MnWO_6 are ideal materials for testing the d^{10}/d^0 effect in the simplest possible system. Both crystallize in the cubic $Fm\bar{3}m$ space group, where the magnetic Mn^{2+} cations form an undistorted face-centered cubic (fcc) lattice. The lattice parameters and bond distances are almost identical due to the similar ionic radii of the $4d^{10}$ Te^{6+} and $5d^0$ W^{6+} cations.[23] Magnetic interactions in these perovskites are three-dimensional unlike in the copper compounds, and there are no quantum effects due to the large, classical-like spin-5/2 on $3d^5$ Mn^{2+} cations. Moreover, there is no spin−orbit coupling nor an orbital moment. As a result, magnetism in both compounds can be described using a simple fcc Heisenberg model with only two interactions as shown in Figure 1: nearest-neighbor J_1 and next-nearest-neighbor J_2 interaction. We have recently reported the full magnetic characterization of Ba_2MnWO_6.[24] The material is cubic with the full ordering of the Mn^{2+} and W^{6+} cations on the B-sites. The space group is $Fm\bar{3}m$ with a = 8.18730(2) at 2 K. The Néel temperature of Ba_2MnWO_6 is 8 K, and it has a Type II antiferromagnetic structure. The J_1 interaction is slightly stronger than the J_2 with J_1 = −0.080 meV and J_2 = −0.076 meV, respectively.

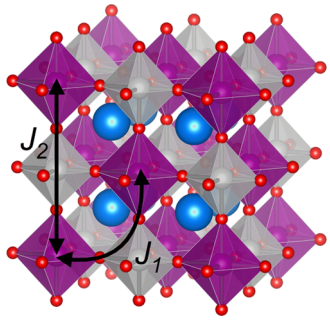

Figure 1. B-site ordered double perovskite structure of Ba_2MnTeO_6 and Ba_2MnWO_6. The A, B′, B″, and O sites are represented by blue, violet, gray, and red spheres, respectively. The main magnetic interactions are shown: nearest-neighbor J_1 (corner to face center) and next-nearest neighbor J_2 (corner to corner).

In this article, we present the magnetic properties of the Mn^{2+} double perovskite Ba_2MnTeO_6 for the first time. Ba_2MnTeO_6 has been synthesized before and a structure was proposed, but its physical properties have not been investigated.[25] It is a $4d^{10}$ Te^{6+} analogue of Ba_2MnWO_6 and allows us to study the effect of d^{10} and d^0 diamagnetic cations on the superexchange interactions in double perovskites. Ba_2MnTeO_6 is isostructural with Ba_2MnWO_6 and crystallizes in the space group $Fm\bar{3}m$ with a = 8.2066(3) at 2 K. Despite minimal differences in crystal structure including bond distances and angles (<0.5%), the magnetic properties of Ba_2MnTeO_6 and Ba_2MnWO_6 are very different. Neutron diffraction experiments reveal a Type I antiferromagnetic structure in Ba_2MnTeO_6 below T_N = 20 K, whereas Ba_2MnWO_6 has a Type II magnetic structure. The main superexchange interaction in Ba_2MnTeO_6 is found to be J_1 = −0.34 meV, while the J_2 interaction is very weak with J_2 = 0.03 meV.

The significant differences in exchange interactions and magnetic structures between these two isostructural compounds can be understood in terms of differences in orbital hybridization between the d^{10} and d^0 cations. We conclude that d^{10} cations on the B″ site in 3d transition metal double perovskites favor antiferromagnetic J_1 interactions, whereas d^0 cations enhance antiferromagnetic J_2 interactions. This is supported by a survey of known ordered double perovskites with either d^{10} Te^{6+} or d^0 W^{6+}/Mo^{6+} cations on the B″-site. This d^{10}/d^0 effect could be used to tune magnetic interactions and ground states in double perovskites in general as has been demonstrated for $Sr_2CuTe_{1-x}W_xO_6$.[13−16] Finally, as in Ba_2MnWO_6, we also observe a short-range correlated magnetic state in Ba_2MnTeO_6 that survives up to $T \approx 5T_N$.

2. EXPERIMENTAL SECTION

2.1. Synthesis. Polycrystalline powder samples of Ba_2MnTeO_6 were prepared using a conventional solid-state chemistry method. Stoichiometric quantities of $BaCO_3$ (99.997%), MnO_2 (99.999%), and TeO_2 (99.9995%) were mixed in an agate mortar, pelletized and calcined at 900 °C in air. The synthesis was carried out in air at 1100 °C for 96 h with intermittent grindings. Phase purity was investigated using X-ray diffraction (Rigaku Miniflex, Cu Kα).

2.2. Physical Characterization. Magnetic properties were measured on a Quantum Design MPMS3 magnetometer. 111.94 mg of sample powder was enclosed in a gelatin capsule, immobilized with polytetrafluoroethylene (PTFE) tape and then placed in a straw sample holder. The measurements were performed in SQUID-VSM mode in the temperature range 2−300 K in an applied field of $\mu_0 H$ = 0.1 T. Both zero-field and field-cooled (FC) measurements were taken. Specific heat was measured with a Quantum Design PPMS instrument using a thermal relaxation method. A 6.84 mg pellet piece was used for the measurements, which were carried out between 2 and 60 K.

2.3. Neutron Powder Diffraction. The nuclear and magnetic structure of Ba_2MnTeO_6 was investigated using neutron diffraction. The measurements were performed on the GEM time-of-flight diffractometer at the ISIS Neutron and Muon Source.[26] Typically, 7.9 g of sample powder was enclosed in a vanadium can. The collected data is available online.[27] Rietveld refinement was carried out using FULLPROF.[28] The crystal structures were visualized using VESTA.[29]

2.4. Inelastic Neutron Scattering. Magnetic excitations in Ba_2MnTeO_6 were measured using time-of-flight inelastic neutron scattering (INS) at the MERLIN instrument[30] at the ISIS Neutron and Muon Source. The same 7.9 g of powder sample was used for both the INS and diffraction experiments. The sample powder was enclosed in an aluminum foil sachet to form an annulus inside a cylindrical aluminum can, which was inserted into a closed-cycle refrigerator to measure between 7 and 200 K. Measurements were performed using a Gd chopper and rep-rate multiplication[31−33] to allow $S(Q,E)$ dynamical structure maps as a function of momentum and energy transfer to be recorded simultaneously with incident energies of 10, 20, and 53 meV. The data were reduced using the MantidPlot software package.[34] The raw data were corrected for detector efficiency and time-independent background following standard procedures. The data sets are available online at ref 35.

2.5. Computational Details. The electronic structures of Ba_2MnTeO_6 and $5d^0$ W^{6+} analogue Ba_2MnWO_6 were calculated using density functional theory (DFT). The calculations were carried out using the full-potential linearized plane-wave (FPLAPW) code ELK.[36] The calculations were performed with generalized gradient approximation functionals by Perdew, Burke, and Ernzerhof[37] (GGA-PBE) with a plane-wave cutoff of $|G + k| = 8/R_{MT}$ au^{-1}, where R_{MT} is the average muffin-tin radius. Electron correlation effects of the localized Mn 3d orbitals were included in a DFT + U approach with the Hubbard U and Hund coupling J as parameters.[38] The calculations were

https://dx.doi.org/10.1021/acs.chemmater.0c02971
Chem. Mater. 2020, 32, 7070−7079

performed with U = 5 and 7 eV with J = 0.9 eV. We used the experimental crystal structures in the calculations with a Type I antiferromagnetic structure, which can be calculated without creating a supercell. While this is not the correct magnetic structure for Ba_2MnWO_6, it has little effect on the density of states, which is our main interest.

3. RESULTS

3.1. Magnetic Properties and Specific Heat. Magnetic properties of Ba_2MnTeO_6 were investigated using DC magnetometry (Figure 2). Two transitions are observed in the zero-field-cooled (ZFC) curve: an antiferromagnetic transition at ≈20 K and a ferro- or ferrimagnetic transition at ≈45 K. The field-cooled (FC) curve diverges from the ZFC curve at the latter transition. The antiferromagnetic transition is inherent to Ba_2MnTeO_6, whereas the latter transition is from a minute Mn_3O_4 impurity not detectable by X-ray diffraction. Mn_3O_4 impurities are common when Mn perovskites are prepared in oxidizing conditions, which for Ba_2MnTeO_6 are needed to oxidize Te^{4+} to Te^{6+}. The Néel temperature of Ba_2MnTeO_6 was determined from the first derivative of $\chi_{mol}T$ vs T curve as T_N = 20.3(2) K.[39]

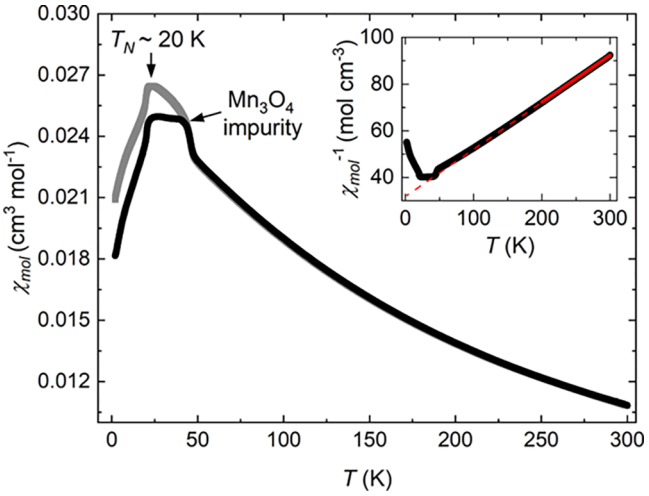

Figure 2. Magnetic susceptibility of Ba_2MnTeO_6. The zero-field-cooled and the field-cooled curves are shown in gray and black, respectively. An antiferromagnetic transition is observed at T_N = 20 K, and a ferrimagnetic transition due to Mn_3O_4 impurity is observed at 45 K. Inset: Inverse magnetic susceptibility and a fit to the Curie–Weiss law yielding Θ_{CW} = −157(1) K and μ_{eff} = 6.30(1) μ_B.

The inverse magnetic susceptibility was fitted to the Curie–Weiss law $\chi_{mol} = C/(T - \Theta_{CW})$ in the temperature range 200–295 K. The Curie–Weiss constant Θ_{CW} gives an estimate of the overall strength of magnetic interactions in a material. For Ba_2MnTeO_6, we obtained Θ_{CW} = −157(1) K indicating strong antiferromagnetic interactions between the $3d^5$ Mn^{2+} cations. The Curie constant was found to be C = 4.96(1) leading to an effective paramagnetic moment of μ_{eff} = 6.30(1) μ_B. This is slightly larger than the expected spin-only value of μ_{SO} = 5.93 μ_B for S = 5/2 Mn^{2+} but is similar to other reported Mn^{2+} double perovskites.[24,40] The degree of magnetic frustration in Ba_2MnTeO_6 was estimated with the frustration factor $f = \Theta_{CW}/T_N \approx 8$, which indicates that the compound is moderately but not strongly frustrated.[41]

The specific heat of Ba_2MnTeO_6 was measured to clarify the magnetic transitions (Figure 3). A single λ anomaly is observed at 20 K indicating a second-order magnetic transition at T_N = 20 K. This confirms that the second feature observed in magnetic susceptibility at 45 K is from a Mn_3O_4 impurity and not intrinsic to Ba_2MnTeO_6. While a small ferrimagnetic impurity can result in a large signal in the magnetic susceptibility, it will not be observed in the specific heat due to the very small change in the overall entropy of the sample.

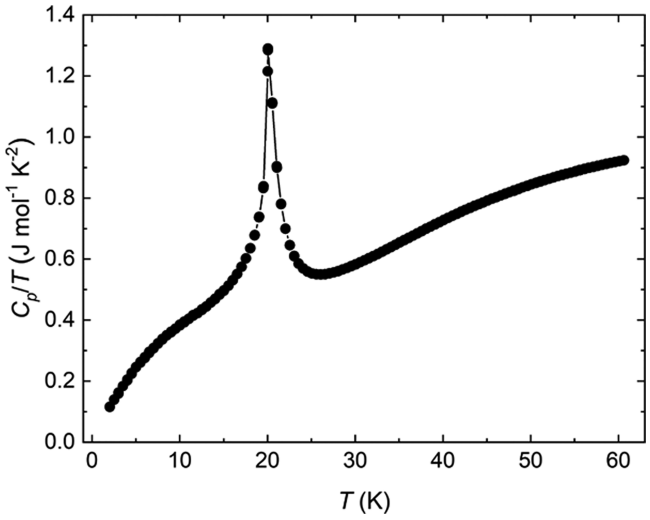

Figure 3. Specific heat of Ba_2MnTeO_6 between 2 and 60 K. The λ anomaly observed at T_N = 20 K is the only magnetic transition in Ba_2MnTeO_6 in this temperature range.

3.2. Crystal Structure. Crystal structures of perovskites can be predicted using the Goldschmidt tolerance factor calculated from the ionic radii of the different cations and the oxygen anion.[1] The tolerance factor for Ba_2MnTeO_6 is t = 1.00 corresponding to the cubic $Fm\bar{3}m$ structure also observed for Ba_2MnWO_6. Te^{6+} double perovskites are generally known to follow the tolerance factor, although they are more likely to form hexagonal perovskite phases than their W^{6+} analogues.[42] Wulff et al.[25] reported the crystal structure of Ba_2MnTeO_6 to be rhombohedrally distorted $R\bar{3}m$ and attributed the distortion to the different sizes of the MnO_6 and TeO_6 octahedra. However, their reported structure is cubic within one standard deviation for both the lattice parameters and atomic positions. To resolve this discrepancy, we performed neutron diffraction measurements at the GEM instrument at the ISIS Neutron and Muon Source.

We found the crystal structure of Ba_2MnTeO_6 to be cubic based on both room-temperature X-ray diffraction and low-temperature (100 K) neutron powder diffraction measurements. All reflections could be indexed in the cubic $Fm\bar{3}m$ space group, and no peak splitting nor anisotropic line broadening expected for a small rhombohedral distortion was observed. The refinement of the 100 K neutron data on the high-resolution bank 6 of GEM is presented in Figure 4. The sample was found to be of high quality with a minor 1.0(1) wt % $BaMnO_3$ impurity, while the trace Mn_3O_4 impurity found in magnetometry could not be observed. The Mn^{2+} and Te^{6+} cations were found to be fully ordered on the two B-sites, and no antisite disorder was observed. This is expected as the B-site cations in Ba_2MnTeO_6 have a large charge difference, which drives the ordering.[1]

For comparison, the refined $Fm\bar{3}m$ structure was transformed to $R\bar{3}m$ using the WYCKSPLIT[43] and TRANSTRU tools provided by the Bilbao Crystallographic Server.[44−46] This space group allows for one additional degree of freedom in the lattice

https://dx.doi.org/10.1021/acs.chemmater.0c02971
Chem. Mater. 2020, 32, 7070−7079

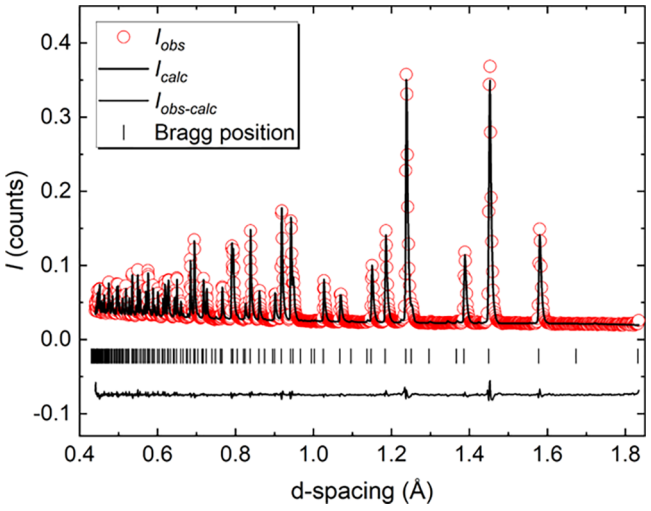

Figure 4. Rietveld refinement of the 100 K neutron diffraction data for Ba_2MnTeO_6 from the high-resolution bank 6 on GEM. The cubic $Fm\bar{3}m$ structure fits very well, and no features suggesting a lower symmetry structure are observed.

parameters, one in the position of barium and one in the position of oxygen. Rietveld refinement in $R\bar{3}m$ leads to only a negligible improvement with the additional positional and lattice parameters remaining within the standard error of their cubic values. This confirms that the structure is indeed cubic (Table 1).

Table 1. Refined Structure of Ba_2MnTeO_6 at 2.1 and 100 K. Space Group $Fm\bar{3}m$ with Ba on (1/4, 1/4, 1/4) Site, Mn on (0, 0, 0) Site, Te on (0, 0, 1/2) Site, and O on (x, 0, 0) Site[a]

	2.1 K	100 K
a (Å)	8.2066(3)	8.2106(4)
Ba 100 × U_{ISO} (Å^2)	0.01(4)	0.13(4)
Mn 100 × U_{ISO} (Å^2)	0.00(4)	0.03(4)
Te 100 × U_{ISO} (Å^2)	0.03(3)	0.07(3)
O x	0.2646(1)	0.2647(1)
O 100 × U_{ISO} (Å^2)	0.22(2)	0.32(2)
$BaMnO_3$ (%)	1.0(1)	1.0(1)
$\boldsymbol{k}$	(0,0,1)	
m_{Mn} (μ_B)	4.34(3)	
R_p (%)	6.61	7.44
R_{wp} (%)	6.47	6.84
R_{exp} (%)	1.89	3.50
χ^2	11.7	3.82

[a]R-factors are reported for the high-resolution backscatter bank 6 (2θ = 153.90°).

3.3. Magnetic Structure. Magnetic Bragg peaks were observed in the neutron diffraction patterns below ≈20 K. These were found to correspond to the propagation vector $\boldsymbol{k}$ = (0,0,1), which is equivalent to $\boldsymbol{k}$ = (1,0,0) = (0,1,0) in $Fm\bar{3}m$. This indicates Type I antiferromagnetic order in Ba_2MnTeO_6. The symmetry-allowed magnetic structures were evaluated using representation analysis with BASIREPS[28] and SARAh.[47] Two irreducible representations were found for the Mn (0,0,0) site in Ba_2MnTeO_6: $\Gamma_{mag} = \Gamma_7 + \Gamma_{10}$. The correct solution Γ_{10} corresponds to ferromagnetic layers of Mn^{2+} cations with in-plane moments stacked antiferromagnetically along c. The other solution Γ_7 has the Mn moment out of plane along c but grossly fails to reproduce the main magnetic peak intensity. The direction of the magnetic moment within the ab plane cannot be determined from powder data. We chose to set it arbitrarily along a. The combined nuclear and magnetic refinement at 2.1 K is shown in Figure 5a. The Type I magnetic structure fits the experimental data well. The higher χ^2 for the 2.1 K refinement is due to an extended counting time compared to the 100 K data set.[48]

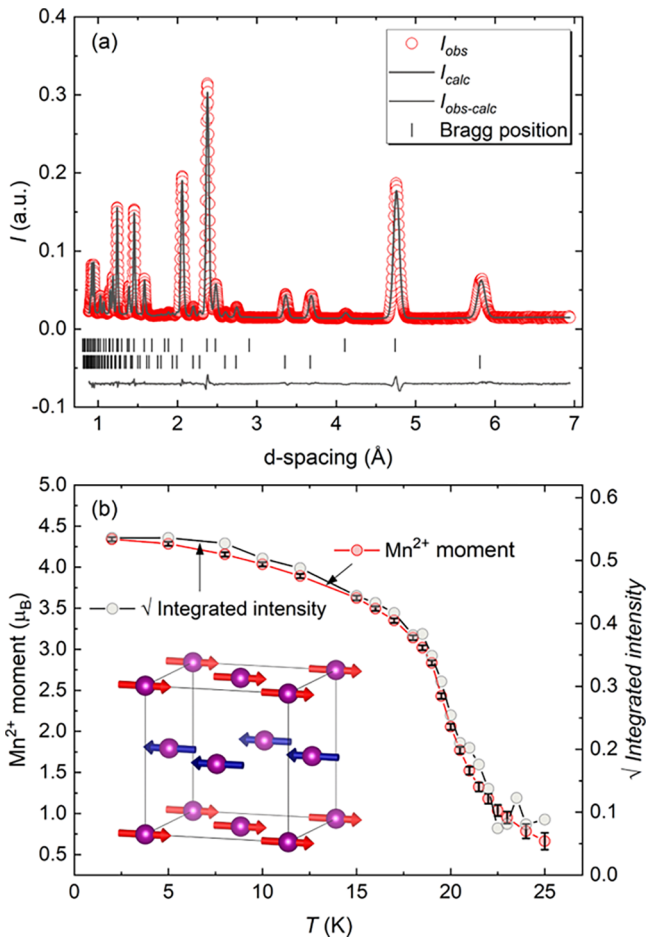

Figure 5. Magnetic refinement. (a) Rietveld refinement of the 2.1 K neutron diffraction data for Ba_2MnTeO_6. The upper bar symbols represent the nuclear phase, while the lower bar symbols mark the positions of the magnetic Bragg reflections. Ba_2MnTeO_6 has the Type I antiferromagnetic structure with a moment of 4.34(3) μ_B at 2.1 K. (b) Thermal evolution of the refined magnetic moment (left) and the square root of the integrated intensity of the main magnetic peak (right). Inset: Magnetic structure of Ba_2MnTeO_6.

The refined magnetic moment of Mn at 2.1 K of 4.34(3) μ_B is as expected for S = 5/2 Mn^{2+}. We have plotted the refined moment as a function of temperature in Figure 5b. At low temperatures, the moment is reduced by spin waves, whereas the reduction in the moment is governed by critical behavior near T_N. The refined moment does not decrease as fast as expected in the critical region. This is likely due to significant diffuse magnetic scattering, which is also observed above T_N. We have plotted the thermal evolution of the square root of the integrated intensity of the main magnetic $(\bar{1}10)$ peak for comparison. Above 22 K, the peak becomes indistinguishable from background, but broad diffuse magnetic scattering remains up to at least 40 K. The magnetic diffuse scattering suggests that a

https://dx.doi.org/10.1021/acs.chemmater.0c02971
Chem. Mater. 2020, 32, 7070−7079

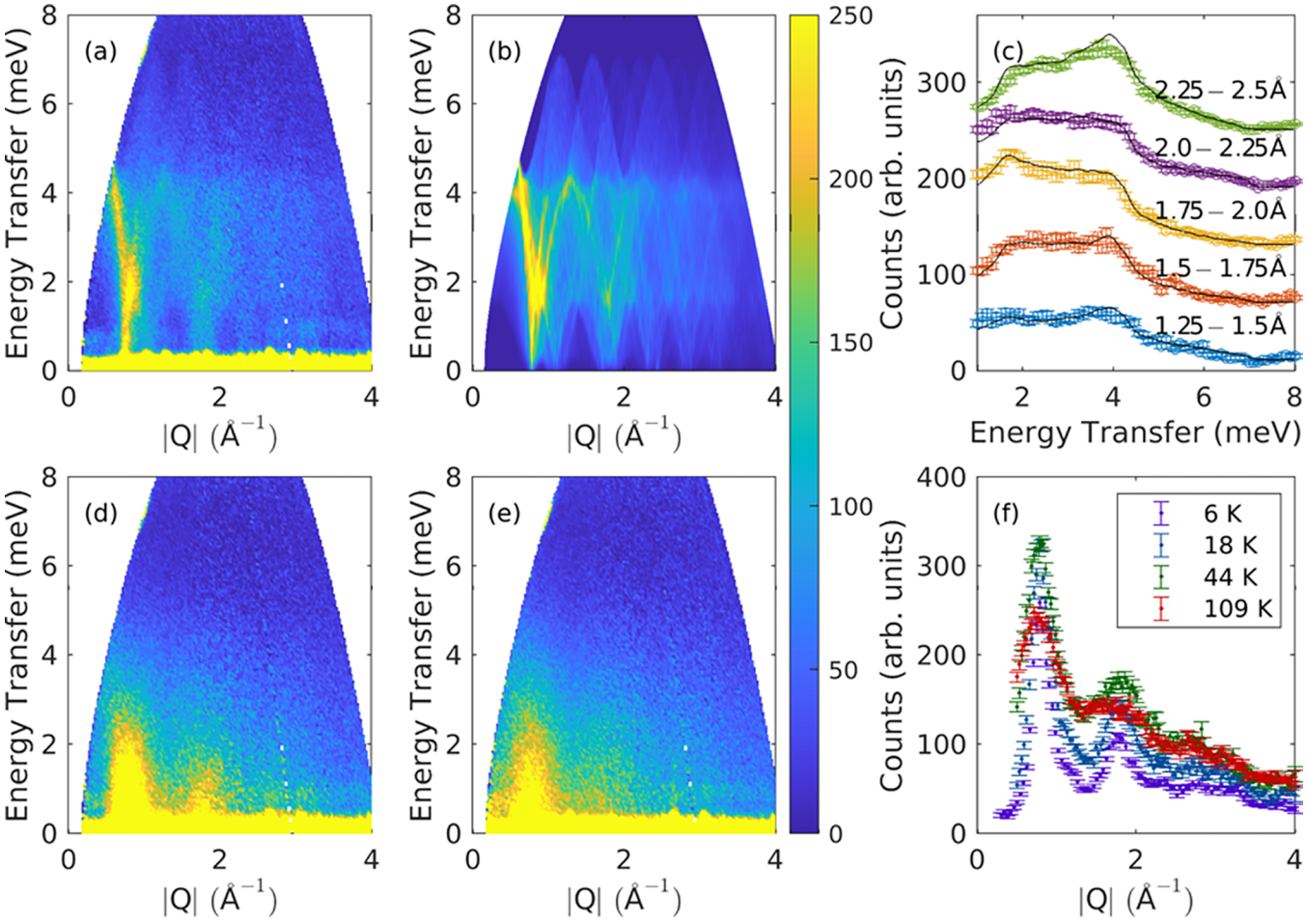

Figure 6. Inelastic neutron scattering from Ba_2MnTeO_6. (a) 7 K data showing clear spin-wave excitations. (b) Spin-wave simulation with $J_1 = -0.34$ and $J_2 = 0.03$ meV. (c) Vertical cuts through the 7 K data summed over different |Q| intervals (squares) and the simulated spectra (black line) confirming that the simulation fits the data well. (d) Data collected at 44 K still show magnetic excitations indicating a short-range correlated magnetic state. (e) Magnetic excitations are observed even at 109 K. (f) Horizontal cuts through the $S(Q,E)$ data summed over $E = 1-2$ meV at different temperatures show that the magnetic excitations observed above $T_N = 20$ K occur at the same positions in |Q|, where the maxima in intensity are observed in the spin-wave spectrum at 7 K.

short-range correlated magnetic state forms above T_N similar to Ba_2MnWO_6.[24]

3.4. Inelastic Neutron Scattering. Magnetic excitations in materials can be investigated using inelastic neutron scattering. For magnetically ordered materials, these excitations are spin waves. Magnetic exchange interactions can then be extracted from the spin-wave spectra using linear spin-wave theory.[49] Inelastic neutron scattering results for Ba_2MnTeO_6 are presented in Figure 6. The data collected at 7 K show clear spin-wave excitations as expected in the magnetically ordered state. The spin-wave spectra were simulated with SpinW.[49] A simple Heisenberg model was sufficient to describe the data

$$H = -J_1 \sum_{(ij)} S_i \cdot S_j - J_2 \sum_{\langle ij \rangle} S_i \cdot S_j \quad (1)$$

where J_1 is the nearest-neighbor interaction, J_2 is the next-nearest-neighbor interaction, $\mathbf{S}_i$ is spin on site i, and the sums are taken over their respective bonds. The spin-wave simulation in Figure 6b reproduces the experimental spectra very well. This is also further supported by the vertical cuts shown in Figure 6c, in which the model closely follows the experimental data. We obtained $J_1 = -0.34$ and $J_2 = 0.03$ meV from the SpinW simulations consistent with the observed Type I antiferromagnetic structure. To conclude, J_1 is the main magnetic interaction in Ba_2MnTeO_6.

Magnetic excitations in Ba_2MnTeO_6 persist far above T_N, as they are observed in the spectra collected at 44 (Figure 6d) and 109 K (Figure 6e). The excitations get weaker with increased temperature and |Q|, which confirms their magnetic origin. The presence of magnetic excitations above T_N indicates that a short-range correlated state forms in Ba_2MnTeO_6. This is consistent with the significant diffuse magnetic scattering observed in the neutron diffraction experiments. This state survives up to at least 109 K, which is over 5 times $T_N = 20$ K. High-temperature short-range correlated magnetic states have also been reported in the double perovskites Ba_2YRuO_6 and Sr_2CuWO_6.[8,50] In Figure 6f, we present horizontal cuts through the data at different temperatures. The cuts show that the magnetic excitations above T_N occur in the same positions in momentum transfer |Q| as the spin waves in the ordered state. This suggests that the short-range correlated state up to $5T_N$ is closely related to the ordered magnetic state below $T_N = 20$ K.

3.5. Electronic Structure. Density functional theory calculations in the DFT + U framework were used to investigate the electronic structures of Ba_2MnTeO_6 and Ba_2MnWO_6. Ba_2MnTeO_6 is an antiferromagnetic insulator as expected with

https://dx.doi.org/10.1021/acs.chemmater.0c02971
Chem. Mater. 2020, 32, 7070−7079

an indirect band gap of E_g = 1.75 eV. The partial density of states for Ba_2MnTeO_6 with U = 7 eV is shown in Figure 7a. The

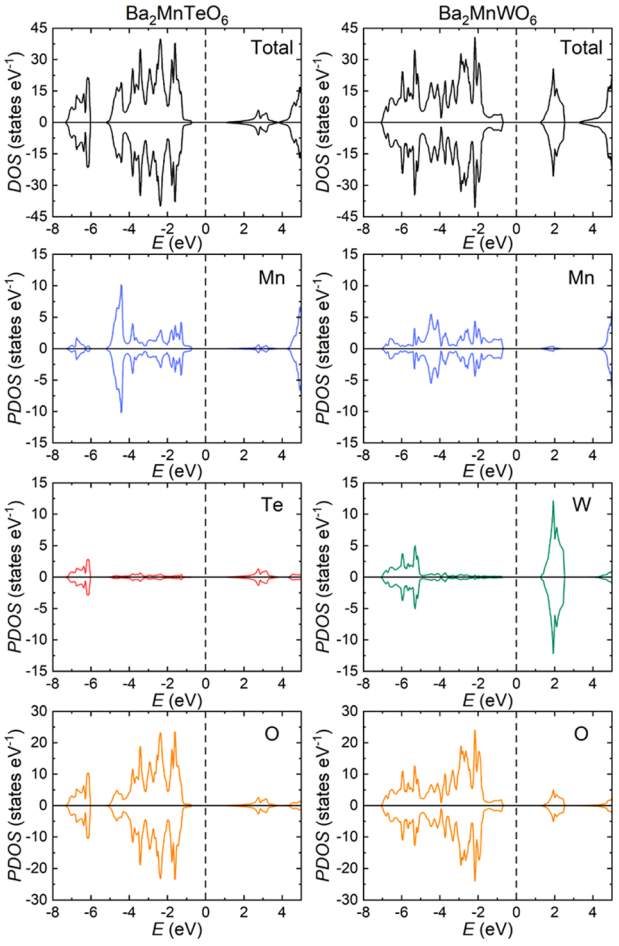

Figure 7. Total and partial density of states of Ba_2MnTeO_6 (a) and Ba_2MnWO_6 (b) calculated within the DFT + U framework with U = 7 eV. The tellurium 5s and 5p states do not significantly hybridize with Mn 3d and O 2p states, whereas W 5d states strongly hybridize with O 2p. This hybridization allows the empty W 5d states to participate in the magnetic interactions.

valence band below the Fermi level consists of hybridized Mn 3d and O 2p states. Similarly, in the conduction band, the empty 3d Mn states hybridize with O 2p states. There is only weak hybridization of the empty Te 5s and 5p states with O 2p or Mn 3d states. The Te $4d^{10}$ states are located significantly below E_F and are not shown. This suggests that tellurium does not participate in the extended superexchange interactions between the Mn^{2+} cations.

Ba_2MnWO_6 is also an antiferromagnetic insulator with E_g = 1.98 eV. The partial density of states, shown in Figure 7b, is different from Ba_2MnTeO_6 in important ways. The conduction band forms from unoccupied W $5d^0$ states, which hybridize strongly with O 2p and, to a lesser degree, Mn 3d states. The valence band is formed of hybridized Mn 3d and O 2p states as in Ba_2MnTeO_6. The strong W $5d^0$−O 2p hybridization indicates that the empty tungsten 5d orbitals participate in the superexchange.

4. DISCUSSION

The typical magnetic structures for B-site ordered double perovskites are the Type I, Type II, and Type III antiferromagnetic order derived from the ground states of the fcc Heisenberg model.[1,51] The Type I structure consists of alternating ferromagnetic layers stacked along [001]. This structure occurs when the antiferromagnetic J_1 interaction dominates, but it is frustrated as only 8 of the 12 nearest-neighbor spins can couple antiferromagnetically. In the Type II structure, alternating ferromagnetic layers are stacked along [111]. In this structure, all of the next-nearest-neighbor spins couple antiferromagnetically, and as such it requires a significant antiferromagnetic J_2 interaction. The type III structure is rare and a mixture of the first two.[1,51] Finally, Néel antiferromagnetic order is observed in some copper double perovskites. In these tetragonal compounds, interactions are strong in the ab plane while out-of-plane interactions are negligible. In the Néel structure, all of the nearest-neighbor in-plane spins couple antiferromagnetically lifting the frustration found in the Type I structure. As such, it requires a dominant J_1 interaction.[52] All of these magnetic structures are visualized in Figure 8.

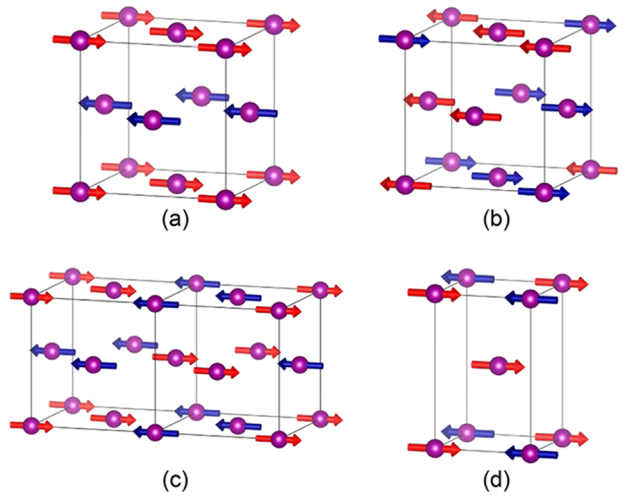

Figure 8. Magnetic structures in double perovskites. (a) Type I antiferromagnetic structure. (b) Type II antiferromagnetic structure. (c) Type III antiferromagnetic structure. (d) Néel antiferromagnetic structure observed in some tetragonal Cu^{2+} double perovskites.

The cubic perovskites Ba_2MnTeO_6 and Ba_2MnWO_6 are isostructural with nearly identical lattice parameters and bond lengths. The only difference in the compounds is the presence of either $4d^{10}$ Te^{6+} or $5d^0$ W^{6+} on the B″-site, which links the extended superexchange pathways between the Mn^{2+} cations. However, this minor difference is enough to result in completely different magnetic interactions and structures: Ba_2MnTeO_6 has the Type I structure with J_1 = −0.34 and J_2 = 0.03 meV, whereas Ba_2MnWO_6 has the Type II structure with J_1 = −0.080 and J_2 = −0.076. Since there are no structural differences, the large change in exchange interactions must be related to a d^{10}/d^0 effect as has been reported for related copper double perovskites.[11−14] This d^{10}/d^0 effect is supported by the density of states plots, where major differences are observed. The Te 5s and 5p states do not significantly hybridize with O 2p states, while $4d^{10}$ orbitals are far below the Fermi level, indicating limited participation of Te in the extended superexchange interactions between Mn cations. In contrast, empty W $5d^0$

https://dx.doi.org/10.1021/acs.chemmater.0c02971
Chem. Mater. 2020, 32, 7070−7079

Table 2. Ordered II−VI Double Perovskites with d^{10} (Te^{6+}) or d^0 (W^{6+}) B″ Cations and Their Magnetic Properties

compound	space group (low T)	T_N (K)	magnetic structure	Θ_{CW} (K)	J_1 (meV)	J_2 (meV)	J_2/J_1	ref
Ba_2MnTeO_6	$Fm\bar{3}m$	20	type I	−157	−0.34	0.03	−0.09	[a]
Sr_2MnTeO_6	$P2_1/n$	20	type I	−136				40
Sr_2CoTeO_6	$P2_1/n$	18	type I	−140				53
Sr_2NiTeO_6	$P2_1/n$	35	type I	−225				54, 55
Ba_2CuTeO_6	$I4/m$		Néel	−400	−20.22	0.23	−0.01	12, 17
Sr_2CuTeO_6	$I4/m$	29	Néel	−80	−7.18	−0.21	0.03	9, 10, 14
Ba_2MnWO_6	$Fm\bar{3}m$	8	type II	−63	−0.080	−0.076	0.95	24
Sr_2MnWO_6	$P2_1/n$	14	type II	−71				56, 57
Sr_2CoWO_6	$P2_1/n$	24	type II	−62				58
Sr_2NiWO_6	$I4/m$	54	type II	−175	−0.02	−1.81	90	55, 59, 60
Ba_2CuWO_6	$I4/m$	28	type II	−249	−1.17	−11.94	10.18	12, 17, 61
Sr_2CuWO_6	$I4/m$	24	type II	−165	−1.2	−9.5	7.92	6−8, 14

[a]This paper.

orbitals strongly hybridize with O 2p orbitals and can therefore participate in the superexchange interactions.

The magnetic ground state of the fcc model is determined by the J_2/J_1 ratio.[51] We will first consider the J_2 interaction, which drives magnetic structure selection as J_1 is antiferromagnetic in both Ba_2MnTeO_6 and Ba_2MnWO_6. J_2 is a 180° Mn−O−B″−O−Mn superexchange interaction. This interaction occurs via the bridging B″ cation, since the O anions are on the opposite sides of the B″ cation and their 2p orbitals are too far away to directly overlap. Since the Te cations do not participate in the superexchange, this interaction is relatively weak in Ba_2MnTeO_6 with $J_2 = 0.03$ meV. The W $5d^0$ orbitals of Ba_2MnWO_6 hybridize with O 2p resulting in a stronger antiferromagnetic $J_2 = -0.076$ meV. The weak ferromagnetic J_2 in Ba_2MnTeO_6 leads to the observed Type I magnetic structure. In Ba_2MnWO_6, the dominant antiferromagnetic J_2 interaction stabilizes the Type II magnetic structure.

The nearest-neighbor J_1 interaction has a 90° Mn−O−B″−O−Mn superexchange pathway. This interaction can occur via overlapping 2p orbitals of the two neighboring oxygens without the participation of the B″ cation and could also be considered as a Mn−O−O−Mn pathway. This is the dominant magnetic interaction in Ba_2MnTeO_6 with $J_1 = -0.34$ meV as Te does not participate in the superexchange. Unexpectedly, the hybridized W $5d^0$ states strongly suppress this interaction in Ba_2MnWO_6 leading to $J_1 = -0.080$ meV, whereas naively one would expect increased hybridization to enhance all exchange interactions. This is not a structural effect as Ba_2MnWO_6 has a slightly smaller lattice parameter, where one would expect slightly stronger magnetic interactions as a result of increased orbital overlap. The J_1 interaction is also strongly suppressed in the related double perovskites Sr_2CuWO_6 and Ba_2CuWO_6.[8,11−13] A thorough analysis of the exchange pathways in Sr_2CuWO_6 revealed that the W $5d^0$ orbitals introduce some ferromagnetic J_1 exchange, which has the overall effect of reducing the antiferromagnetic J_1 exchange mainly occurring via the overlapping O 2p orbitals.[13] This is the likely origin of the suppression of J_1 in Ba_2MnWO_6 as well, although confirmation would require more advanced ab initio calculations. The strong suppression of J_1 naturally explains why Ba_2MnTeO_6 has a higher T_N and more negative Θ_{CW} than Ba_2MnWO_6 as J_1 is suppressed more than J_2 is enhanced.

For comparison, in Table 2, we have collected crystallographic and magnetic data for $A_2MB''O_6$ double perovskites, where M is a divalent 3d transition metal cation and B″ is Te^{6+} or W^{6+}. We have only included compounds where both the Te^{6+} and W^{6+} analogues form an ordered double perovskite. The monoclinic $P2_1/n$ Sr_2MnTeO_6 and Sr_2MnWO_6 behave similarly to the barium analogues such that the former has the Type I structure while the latter has Type II.[40,56,57] All of the compounds with a d^{10} Te^{6+} linking B″ cation have either Type I or Néel antiferromagnetic structures, revealing dominant antiferromagnetic J_1 interactions. In contrast, all of the d^0 W^{6+} analogues have Type II antiferromagnetic order indicating significant antiferromagnetic J_2 interactions. While we have limited our discussion here to Te^{6+} and W^{6+} double perovskites due to their near-identical ionic radii, the same Type II antiferromagnetic structure observed in $5d^0$ W^{6+} compounds is also found in the corresponding $4d^0$ Mo^{6+} materials including Ba_2MnMoO_6.[6,57,62−65] This further supports that the differences in magnetic structures and interactions are driven by a d^{10}/d^0 effect.

We can make two main conclusions based on the observed magnetic structures. (1) d^{10} cations on the B″-site promote strong antiferromagnetic J_1 interactions leading to Type I or Néel magnetic structures. The Type I antiferromagnetic structure is only possible when J_1 is antiferromagnetic and J_2 is ferromagnetic. Since the Curie−Weiss constant, Θ_{CW}, is negative for all listed Te^{6+} compounds, the antiferromagnetic J_1 is much stronger than the ferromagnetic J_2 in these compounds. (2) d^0 cations on the B″-site promote antiferromagnetic J_2 interactions leading to Type II magnetic structures such that $J_2/J_1 > 0.5$, while J_1 also remains antiferromagnetic. For some Type II compounds where the interactions are known, the antiferromagnetic J_2 is dominant; but for Ba_2MnWO_6, it is of the same order as J_1. These rules open up the possibility of tuning magnetic interactions in double perovskites by making substitutions on the B″-site. This effect has already been demonstrated in the Cu^{2+} double perovskite series $Sr_2CuTe_{1-x}W_xO_6$, where the ground state can be tuned from Néel order to a spin-liquid-like state to Type II order as a function of x.[14,15]

It is not presently known how widely the d^{10}/d^0 rules established here are applicable to other B-site ordered transition metal double perovskites with d^{10} and d^0 B″ cations. It should be noted that other factors such as the degree of cation ordering and octahedral tilting also affect the magnetism in double perovskites. Sr_2FeSbO_6 with partial cation ordering of Fe^{3+} and the d^0 Sb^{5+}, for instance, does have the expected Type I structure, but the B-sites are disordered in the Nb^{5+} and Ta^{5+} d^0 analogues leading to spin glass states.[66,67] Similarly, Sr_2CrSbO_6 is a Type I antiferromagnet while the more distorted Ca_2CrSbO_6

https://dx.doi.org/10.1021/acs.chemmater.0c02971
Chem. Mater. 2020, 32, 7070−7079

with larger octahedral tilting becomes ferromagnetic.[68] $SrLaNiSbO_6$ and $BaLaCuSbO_6$ have the expected Type I and Néel magnetic structures, respectively.[69,70]

The d^{10}/d^0 effect explains the observed magnetic structures in a large number of 3d transition metal double perovskites. This does not appear to be the case for 4d and 5d double perovskites, which have significant spin−orbit coupling and reduced on-site Coulombic repulsion compared to 3d transition metals. A number of $4d^3$ Ru^{5+} and $5d^3$ Os^{5+} double perovskites with d^0 B″ cations including Ba_2YRuO_6, Ba_2YOsO_6, and Sr_2YOsO_6 have Type I magnetic order instead of the expected Type II order.[18−21]

A computational study comparing the d^{10} double perovskite Sr_2InOsO_6 to its d^0 analogues Sr_2ScOsO_6 and Sr_2YOsO_6 found a connection between d^0 orbital hybridization and the overall strength of magnetic interactions and T_N.[21] All three of these compounds have the Type I antiferromagnetic structure, but calculated J values show that each of these interactions in the d^{10} Sr_2ScOsO_6 is much weaker than in its d^0 analogues. We note that the calculations of the Sr_2MOsO_6 system do not reproduce the observed magnetic ground state without the inclusion of spin−orbit coupling. This confirms the crucial role of spin−orbit coupling in the electronic properties of these 5d materials. The difference in the behavior of the 3d transition metal double perovskites is likely related to the absence of significant spin−orbit coupling.[18]

The d^{10}/d^0 effect in the osmates is the opposite of observations in the 3d transition metal double perovskites investigated here, where Te^{6+} d^{10} compounds tend to have stronger magnetic interactions than the W^{6+} d^0 compounds. In these tungstates, J_1 is strongly suppressed while J_2 is increased leading to a decrease in the overall strength of interactions. Hence, in the 3d transition metal compounds, the d^{10}/d^0 effect changes the dominant antiferromagnetic interaction from J_1 to J_2.

5. CONCLUSIONS

We have characterized the magnetic properties of the *B*-site ordered double perovskite Ba_2MnTeO_6. It has a cubic $Fm\bar{3}m$ structure with a = 8.2066(3) Å at 2 K. The compound orders magnetically at T_N = 20 K in the Type I antiferromagnetic structure and has a Curie−Weiss temperature of −157(1) K indicating significant antiferromagnetic interactions. The exchange constants were extracted from inelastic neutron scattering data. Magnetism in Ba_2MnTeO_6 is well described by a fcc Heisenberg model with two interactions: nearest-neighbor J_1 = −0.34 meV and next-nearest-neighbor J_2 = 0.03 meV. A short-range correlated magnetic state was observed at high temperatures up to $T \approx 5T_N$.

Ba_2MnTeO_6 and its tungsten analogue Ba_2MnWO_6 are excellent materials for testing the effects of filled shell d^{10} (Te^{6+}) and empty shell d^0 (W^{6+}) bridging B″-site cations on magnetic interactions in perovskites. The compounds are isostructural with very similar lattice parameters due to the similar ionic radii of Te^{6+} and W^{6+}. The magnetic structures and interactions in these compounds are very different: Ba_2MnTeO_6 has the Type I structure with a dominant J_1 interaction, while Ba_2MnWO_6 has the Type II structure with a significant antiferromagnetic J_2 interaction. This arises due to differences in the orbital hybridization with oxygen. The empty W d^0 states hybridize strongly with oxygen 2p states, and consequently tungsten participates in the next-nearest-neighbor extended superexchange pathway enabling a significant J_2 interaction. In contrast, the filled d^{10} Te states are far below the Fermi level, while the empty s and p orbitals hybridize only weakly with O 2p. This leads to a very weak J_2 interaction, while J_1 dominates. This d^{10}/d^0 effect, where d^{10} cations in the bridging B″ sites promote J_1 interactions and d^0 B″ cations promote J_2 interactions, is also observed in other B-site ordered double perovskites with 3d transition metals as the magnetic cation. Magnetic interactions in 3d double perovskites could be tuned by substituting d^{10}/d^0 cations on the B″-site. Magnetic 4d and 5d systems do not follow these trends due to significant spin−orbit coupling.

■ ASSOCIATED CONTENT

Supporting Information

The Supporting Information is available free of charge at https://pubs.acs.org/doi/10.1021/acs.chemmater.0c02971.

Rietveld refinement *R*-factors, bond valence sums, laboratory X-ray diffraction, low-temperature neutron diffraction, density of states comparison (PDF)

Crystallographic data 2 K (CIF)

Crystallographic data 100 K (CIF)

■ AUTHOR INFORMATION

Corresponding Author

Edmund J. Cussen − *Department of Material Science and Engineering, University of Sheffield, Sheffield S1 3JD, United Kingdom*; orcid.org/0000-0002-2899-6888; Email: e.j.cussen@sheffield.ac.uk

Authors

Otto H. J. Mustonen − *Department of Material Science and Engineering, University of Sheffield, Sheffield S1 3JD, United Kingdom*

Charlotte E. Pughe − *Department of Material Science and Engineering, University of Sheffield, Sheffield S1 3JD, United Kingdom*

Helen C. Walker − *ISIS Pulsed Neutron and Muon Source, STFC Rutherford Appleton Laboratory, Didcot OX11 0QX, United Kingdom*

Heather M. Mutch − *Department of Material Science and Engineering, University of Sheffield, Sheffield S1 3JD, United Kingdom*

Gavin B. G. Stenning − *ISIS Pulsed Neutron and Muon Source, STFC Rutherford Appleton Laboratory, Didcot OX11 0QX, United Kingdom*

Fiona C. Coomer − *Johnson Matthey Battery Materials, Reading RG4 9NH, United Kingdom*

Complete contact information is available at: https://pubs.acs.org/10.1021/acs.chemmater.0c02971

Notes

The authors declare no competing financial interest.

■ ACKNOWLEDGMENTS

This work was funded by the Leverhulme Trust Research Project Grant RPG-2017-109. Dr. Ivan da Silva is thanked for assistance with the neutron diffraction measurements. Dr. Alex Gibbs is thanked for helpful discussions. The authors are grateful to the Science and Technology Facilities Council for the beamtime allocated at ISIS. The authors are thankful for access to the MPMS3 and PPMS instruments at the Materials Characterisation Laboratory at ISIS.

■ ABBREVIATIONS

fcc, face-centered cubic; MPMS, magnetic property measurement system; SQUID, superconducting quantum interference device; VSM, vibrating sample magnetometer; PPMS, physical property measurement system; PTFE, polytetrafluoroethylene; INS, inelastic neutron scattering; DFT, density functional theory; FPLAPW, full-potential linearized plane-wave; GGA, generalized gradient approximation; PBE, functionals by Perdew, Burke, and Ernzerhof; ZFC, zero-field-cooled; FC, field-cooled

■ REFERENCES

(1) Vasala, S.; Karppinen, M. $A_2B'B''O_6$ Perovskites: A Review. *Prog. Solid State Chem.* **2015**, *43*, 1−36.

(2) Goodenough, J. B. Theory of the Role of Covalence in the Perovskite-Type Manganites [La,M(II)]MnO_3. *Phys. Rev.* **1955**, *100*, 564−573.

(3) Goodenough, J. B. An Interpretation of the Magnetic Properties of the Perovskite-Type Mixed Crystals $La_{1-x}Sr_xCoO_{3-\lambda}$. *J. Phys. Chem. Solids* **1958**, *6*, 287−297.

(4) Kanamori, J. Superexchange Interaction and Symmetry Properties of Electron Orbitals. *J. Phys. Chem. Solids* **1959**, *10*, 87−98.

(5) Zhu, M.; Do, D.; Dela Cruz, C. R.; Dun, Z.; Zhou, H. D.; Mahanti, S. D.; Ke, X. Tuning the Magnetic Exchange via a Control of Orbital Hybridization in $Cr_2(Te_{1-x}W_x)O_6$. *Phys. Rev. Lett.* **2014**, *113*, No. 076406.

(6) Vasala, S.; Saadaoui, H.; Morenzoni, E.; Chmaissem, O.; Chan, T.; Chen, J.; Hsu, Y.; Yamauchi, H.; Karppinen, M. Characterization of Magnetic Properties of Sr_2CuWO_6 and Sr_2CuMoO_6. *Phys. Rev. B* **2014**, *89*, No. 134419.

(7) Vasala, S.; Avdeev, M.; Danilkin, S.; Chmaissem, O.; Karppinen, M. Magnetic Structure of Sr_2CuWO_6. *J. Phys.: Condens. Matter* **2014**, *26*, No. 496001.

(8) Walker, H. C.; Mustonen, O.; Vasala, S.; Voneshen, D. J.; Le, M. D.; Adroja, D. T.; Karppinen, M. Spin Wave Excitations in the Tetragonal Double Perovskite Sr_2CuWO_6. *Phys. Rev. B* **2016**, *94*, No. 064411.

(9) Koga, T.; Kurita, N.; Avdeev, M.; Danilkin, S.; Sato, T. J.; Tanaka, H. Magnetic Structure of the S = 1/2 Quasi-Two-Dimensional Square-Lattice Heisenberg Antiferromagnet Sr_2CuTeO_6. *Phys. Rev. B* **2016**, *93*, No. 054426.

(10) Babkevich, P.; Katukuri, V. M.; Fåk, B.; Rols, S.; Fennell, T.; Pajić, D.; Tanaka, H.; Pardini, T.; Singh, R. R. P.; Mitrushchenkov, A.; Yazyev, O. V.; Rønnow, H. M. Magnetic Excitations and Electronic Interactions in Sr_2CuTeO_6: A Spin-1/2 Square Lattice Heisenberg Antiferromagnet. *Phys. Rev. Lett.* **2016**, *117*, No. 237203.

(11) Xu, Y.; Liu, S.; Qu, N.; Cui, Y.; Gao, Q.; Chen, R.; Wang, J.; Gao, F.; Hao, X. Comparative Description of Magnetic Interactions in Sr_2CuTeO_6 and Sr_2CuWO_6. *J. Phys.: Condens. Matter* **2017**, *29*, No. 105801.

(12) Mustonen, O.; Vasala, S.; Mutch, H.; Thomas, C. I.; Stenning, G. B. G.; Baggio-Saitovitch, E.; Cussen, E. J.; Karppinen, M. Magnetic Interactions in the S = 1/2 Square-Lattice Antiferromagnets Ba_2CuTeO_6 and Ba_2CuWO_6: Parent Phases of a Possible Spin Liquid. *Chem. Commun.* **2019**, *55*, 1132−1135.

(13) Katukuri, V. M.; Babkevich, P.; Mustonen, O.; Walker, H. C.; Fåk, B.; Vasala, S.; Karppinen, M.; Rønnow, H. M.; Yazyev, O. V. Exchange Interactions Mediated by Non-Magnetic Cations in Double Perovskites. *Phys. Rev. Lett.* **2020**, *124*, No. 077202.

(14) Mustonen, O.; Vasala, S.; Sadrollahi, E.; Schmidt, K. P.; Baines, C.; Walker, H. C.; Terasaki, I.; Litterst, F. J.; Baggio-Saitovitch, E.; Karppinen, M. Spin-Liquid-like State in a Spin-1/2 Square-Lattice Antiferromagnet Perovskite Induced by d^{10}−d^0 Cation Mixing. *Nat. Commun.* **2018**, *9*, No. 1085.

(15) Mustonen, O.; Vasala, S.; Schmidt, K. P.; Sadrollahi, E.; Walker, H. C.; Terasaki, I.; Litterst, F. J.; Baggio-Saitovitch, E.; Karppinen, M. Tuning the S = 1/2 Square-Lattice Antiferromagnet $Sr_2Cu(Te_{1-x}W_x)O_6$ from Néel Order to Quantum Disorder to Columnar Order. *Phys. Rev. B* **2018**, *98*, No. 064411.

(16) Watanabe, M.; Kurita, N.; Tanaka, H.; Ueno, W.; Matsui, K.; Goto, T. Valence-Bond-Glass State with a Singlet Gap in the Spin-1/2 Square-Lattice Random J_1-J_2 Heisenberg Antiferromagnet $Sr_2CuTe_{1-x}W_xO_6$. *Phys. Rev. B* **2018**, *98*, No. 054422.

(17) Iwanaga, D.; Inaguma, Y.; Itoh, M. Crystal Structure and Magnetic Properties of B-Site Ordered Perovskite-Type Oxides $A_2CuB'O_6$ (A = Ba, Sr; B′ = W, Te). *J. Solid State Chem.* **1999**, *147*, 291−295.

(18) Maharaj, D. D.; Sala, G.; Marjerrison, C. A.; Stone, M. B.; Greedan, J. E.; Gaulin, B. D. Spin Gaps in the Ordered States of La_2LiXO_6 (X=Ru,Os) and Their Relation to the Distortion of the Cubic Double Perovskite Structure in $4d^3$ and $5d^3$ Magnets. *Phys. Rev. B* **2018**, *98*, No. 104434.

(19) Paul, A. K.; Sarapulova, A.; Adler, P.; Reehuis, M.; Kanungo, S.; Mikhailova, D.; Schnelle, W.; Hu, Z.; Kuo, C.; Siruguri, V.; Rayaprol, S.; Soo, Y.; Yan, B.; Felser, C.; Tjeng, L. H.; Jansen, M. Magnetically Frustrated Double Perovskites: Synthesis, Structural Properties, and Magnetic Order of Sr_2BOsO_6 (B = Y, In, Sc). *Z. Anorg. Allg. Chem.* **2015**, *641*, 197−205.

(20) Taylor, A. E.; Morrow, R.; Singh, D. J.; Calder, S.; Lumsden, M. D.; Woodward, P. M.; Christianson, A. D. Magnetic Order and Electronic Structure of the 5d3 Double Perovskite Sr_2ScOsO_6. *Phys. Rev. B* **2015**, *91*, No. 100406.

(21) Kanungo, S.; Yan, B.; Felser, C.; Jansen, M. Active Role of Nonmagnetic Cations in Magnetic Interactions for Double-Perovskite Sr_2BOsO_6 (B = Y, In, Sc). *Phys. Rev. B* **2016**, *93*, No. 161116.

(22) Marjerrison, C. A.; Thompson, C. M.; Sharma, A. Z.; Hallas, A. M.; Wilson, M. N.; Munsie, T. J. S.; Flacau, R.; Wiebe, C. R.; Gaulin, B. D.; Luke, G. M.; Greedan, J. E. Magnetic Ground States in the Three Os^{6+} ($5d^2$) Double Perovskites Ba_2MOsO_6 (M = Mg, Zn, and Cd) from Néel Order to Its Suppression. *Phys. Rev. B* **2016**, *94*, No. 134429.

(23) Shannon, R. D. Revised Effective Ionic Radii and Systematic Studies of Interatomic Distances in Halides and Chalcogenides. *Acta Crystallogr., Sect. A: Cryst. Phys., Diffr., Theor. Gen. Crystallogr.* **1976**, *32*, 751−767.

(24) Mutch, H.; Mustonen, O.; Walker, H. C.; Baker, P. J.; Stenning, G. B. G.; Coomer, F. C.; Cussen, E. J. Long- and Short-Range Magnetism in the Frustrated Double Perovskite Ba_2MnWO_6. *Phys. Rev. Mater.* **2020**, *4*, No. 014408.

(25) Wulff, L.; Wedel, B.; Müller-Buschbaum, H. Zur Kristallchemie von Telluraten Mit Mn^{2+} Im Kationischen Und Anionischen Teil Kristallstruktur: $(Mn_{2,4}Cu_{0,6})TeO_6$, Ba_2MnTeO_6 and $Pb(Mn_{0,5}Te_{0,5})O_3$. *Z. Naturforsch. B* **1998**, *53*, 49−52.

(26) Williams, W. G.; Ibberson, R. M.; Day, P.; Enderby, J. E. GEM - General Materials Diffractometer at ISIS. *Phys. B* **1997**, *241*−*243*, 234−236.

(27) Cussen, E. J.; da Silva, I.; Mutch, H.; Mustonen, O.; Pughe, C. Magnetic Frustration on the Face-Centred Lattice of Ba_2MnTeO_6, STFC ISIS Neutron and Muon Source, 2019. https://doi.org/10.5286/ISIS.E.RB1910507.

(28) Rodríguez-Carvajal, J. Recent Advances in Magnetic Structure Determination by Neutron Powder Diffraction. *Phys. B* **1993**, *192*, 55−69.

(29) Momma, K.; Izumi, F. VESTA 3 for Three-Dimensional Visualization of Crystal, Volumetric and Morphology Data. *J. Appl. Crystallogr.* **2011**, *44*, 1272−1276.

(30) Bewley, R. I.; Guidi, T.; Bennington, S. *MERLIN: A High Count Rate Chopper Spectrometer at ISIS*; Notiziario Neutroni e Luce di Sincrotrone, 2009; Vol. *14*, pp 22−27.

(31) Russina, M.; Mezei, F. First Implementation of Repetition Rate Multiplication in Neutron Spectroscopy. *Nucl. Instrum. Methods Phys. Res., Sect. A* **2009**, *604*, 624−631.

(32) Russina, M.; Mezei, F. Implementation of Repetition Rate Multiplication in Cold, Thermal and Hot Neutron Spectroscopy. *J. Phys. Conf. Ser.* **2010**, *251*, No. 012079.

(33) Nakamura, M.; Kajimoto, R.; Inamura, Y.; Mizuno, F.; Fujita, M.; Yokoo, T.; Arai, M. First Demonstration of Novel Method for Inelastic

https://dx.doi.org/10.1021/acs.chemmater.0c02971
Chem. Mater. 2020, 32, 7070−7079

Neutron Scattering Measurement Utilizing Multiple Incident Energies. *J. Phys. Soc. Jpn.* **2009**, *78*, No. 093002.
(34) Arnold, O.; Bilheux, J. C.; Borreguero, J. M.; Buts, A.; Campbell, S. I.; Chapon, L.; Doucet, M.; Draper, N.; Ferraz Leal, R.; Gigg, M. A.; Lynch, V. E.; Markvardsen, A.; Mikkelson, D. J.; Mikkelson, R. L.; Miller, R.; Palmen, K.; Parker, P.; Passos, G.; Perring, T. G.; Peterson, P. F.; Ren, S.; Reuter, M. A.; Savici, A. T.; Taylor, J. W.; Taylor, R. J.; Tolchenov, R.; Zhou, W.; Zikovsky, J. Mantid - Data Analysis and Visualization Package for Neutron Scattering and μSR Experiments. *Nucl. Instrum. Methods Phys. Res., Sect. A* **2014**, *764*, 156−166.
(35) Walker, H. C. Spin Wave Investigation of Ba_2MnWO_6 and Ba_2MnTeO_6, STFC ISIS Neutron and Muon Source, 2019. https://doi.org/10.5286/ISIS.E.RB1890354.
(36) The Elk Code. http://elk.sourceforge.net (accessed July 1, 2020).
(37) Perdew, J. P.; Burke, K.; Ernzerhof, M. Generalized Gradient Approximation Made Simple. *Phys. Rev. Lett.* **1996**, *77*, 3865−3868.
(38) Liechtenstein, A. I.; Anisimov, V. I.; Zaanen, J. Density-Functional Theory and Strong Interactions: Orbital Ordering in Mott-Hubbard Insulators. *Phys. Rev. B* **1995**, *52*, R5467−R5470.
(39) Bragg, E. E.; Seehra, M. S. Magnetic Susceptibility of MnF_2 near T_N and Fisher's Relation. *Phys. Rev. B* **1973**, *7*, 4197−4202.
(40) Ortega-San Martin, L.; Chapman, J. P.; Lezama, L.; Sánchez Marcos, J.; Rodríguez-Fernández, J.; Arriortua, M. I.; Rojo, T. Magnetic Properties of the Ordered Double Perovskite Sr_2MnTeO_6. *Eur. J. Inorg. Chem.* **2006**, *2006*, 1362−1370.
(41) Greedan, J. E. Geometrically Frustrated Magnetic Materials. *J. Mater. Chem.* **2001**, *11*, 37−53.
(42) Flores, A. V.; Krueger, A. E.; Stiner, A. J.; Albert, H. M.; Mansur, T.; Willis, V.; Lee, C. C.; Garay, L. J.; Nguyen, L. T.; Frank, M. A.; Barnes, P. W.; Fry-Petit, A. M. Comparison of the Crystal Chemistry of Tellurium (VI), Molybdenum (VI), and Tungsten (VI) in Double Perovskite Oxides and Related Materials. *Prog. Solid State Chem.* **2019**, *56*, No. 100251.
(43) Kroumova, E.; Perez-Mato, J. M.; Aroyo, M. I. Wycksplit: A Computer Program for Determination of the Relations of Wyckoff Positions for a Group-Subgroup Pair. *J. Appl. Crystallogr.* **1998**, *31*, 646.
(44) Aroyo, M. I.; Perez-Mato, J. M.; Capillas, C.; Kroumova, E.; Ivantchev, S.; Madariaga, G.; Kirov, A.; Wondratschek, H. Bilbao Crystallographic Server: I. Databases and Crystallographic Computing Programs. *Z. Kristallogr. - Cryst. Mater.* **2006**, *221*, 15−27.
(45) Aroyo, M. I.; Kirov, A.; Capillas, C.; Perez-Mato, J. M.; Wondratschek, H. Bilbao Crystallographic Server. II. Representations of Crystallographic Point Groups and Space Groups. *Acta Crystallogr., Sect. A: Found. Crystallogr.* **2006**, *62*, 115−128.
(46) Aroyo, M. I.; Perez-Mato, J. M.; Orobengoa, D.; Tasci, E. De La Flor, G.; Kirov, A. Crystallography Online: Bilbao Crystallographic Server. *Bulg. Chem. Commun.* **2011**, *43*, 183−197.
(47) Wills, A. S. New Protocol for the Determination of Magnetic Structures Using Simulated Annealing and Representational Analysis (SARAh). *Phys. B* **2000**, *276−278*, 680−681.
(48) Toby, B. H. R. Factors in Rietveld Analysis: How Good Is Good Enough? *Powder Diffr.* **2006**, *21*, 67−70.
(49) Toth, S.; Lake, B. Linear Spin Wave Theory for Single-Q Incommensurate Magnetic Structures. *J. Phys.: Condens. Matter* **2015**, *27*, No. 166002.
(50) Nilsen, G. J.; Thompson, C. M.; Ehlers, G.; Marjerrison, C. A.; Greedan, J. E. Diffuse Magnetic Neutron Scattering in the Highly Frustrated Double Perovskite Ba_2YRuO_6. *Phys. Rev. B: Condens. Matter Mater. Phys.* **2015**, *91*, No. 054415.
(51) Sun, N. N.; Wang, H. Y. The J_1-J_2model on the Face-Centered-Cubic Lattices. *J. Magn. Magn. Mater.* **2018**, *454*, 176−184.
(52) Mikheyenkov, A. V.; Shvartsberg, A. V.; Valiulin, V. E.; Barabanov, A. F. Thermodynamic Properties of the 2D Frustrated Heisenberg Model for the Entire J_1-J_2 Circle. *J. Magn. Magn. Mater.* **2016**, *419*, 131−139.
(53) Ortega-San Martin, L.; Chapman, J. P.; Lezama, L.; Sánchez-Marcos, J.; Rodríguez-Fernández, J.; Arriortua, M. I.; Rojo, T. Factors Determining the Effect of Co(II) in the Ordered Double Perovskite Structure: Sr_2CoTeO_6. *J. Mater. Chem.* **2005**, *15*, 183−193.
(54) Orayech, B.; Ortega-San-Martín, L.; Urcelay-Olabarria, I.; Lezama, L.; Rojo, T.; Arriortua, M.; Igartua, J. M. Effect of Partial Substitution of Ni by Mg on the Structural, Magnetic and Spectroscopic Properties of the Double Perovskite Sr_2NiTeO_6. *Dalton Trans.* **2016**, *45*, 14378−14393.
(55) Iwanaga, D.; Inaguma, Y.; Itoh, M. Structure and Magnetic Properties of Sr_2NiAO_6 (A = W, Te). *Mater. Res. Bull.* **2000**, *35*, 449−457.
(56) Azad, A. K.; Ivanov, S.; Eriksson, S. G.; Rundlöf, H.; Eriksen, J.; Mathieu, R.; Svedlindh, P. Structural and Magnetic Properties of the Double Perovskite Sr_2MnWO_6. *J. Magn. Magn. Mater.* **2001**, *237*, 124−134.
(57) Muñoz, A.; Alonso, J. A.; Casais, M. T.; Martínez-Lope, M. J.; Fernández-Díaz, M. T. Crystal and Magnetic Structure of the Compelx Oxides Sr_2MnMoO_6, Sr_2MnWO_6 and Ca_2MnWO_6: A Neutron Diffraction Study. *J. Phys.: Condens. Matter* **2002**, *14*, 8817−8830.
(58) Viola, M. C.; Martínez-Lope, M. J.; Alonso, J. A.; Martínez, J. L.; De Paoli, J. M.; Pagola, S.; Pedregosa, J. C.; Fernández-Díaz, M. T.; Carbonio, R. E. Structure and Magnetic Properties of Sr_2CoWO_6: An Ordered Double Perovskite Containing Co^{2+}(HS) with Unquenched Orbital Magnetic Moment. *Chem. Mater.* **2003**, *15*, 1655−1663.
(59) Todate, Y. Exchange Interactions in Antiferromagnetic Complex Perovskites. *J. Phys. Chem. Solids* **1999**, *60*, 1173−1175.
(60) Rezaei, N.; Hashemifar, T.; Alaei, M.; Shahbazi, F.; Hashemifar, S. J.; Akbarzadeh, H. Ab Initio Investigation of Magnetic Ordering in the Double Perovskite Sr_2NiWO_6. *Phys. Rev. B* **2019**, *99*, No. 104411.
(61) Todate, Y.; Higemoto, W.; Nishiyama, K.; Hirota, K. Magnetic Ordering in Ordered Complex Cu Perovskite Probed by μSR and Neutron Diffraction. *J. Phys. Chem. Solids* **2007**, *68*, 2107−2110.
(62) Martínez-Lope, M. J.; Alonso, J. A.; Casais, M. T. Synthesis, Crystal and Magnetic Structure of the Double Perovskites A_2NiMoO_6 (A = Sr, Ba): A Neutron Diffraction Study. *Eur. J. Inorg. Chem.* **2003**, *6*, 2839−2844.
(63) Eriksson, A. K.; Eriksson, S. G.; Ivanov, S. A.; Knee, C. S.; Eriksen, J.; Rundlöf, H.; Tseggai, M. High Temperature Phase Transition of the Magnetoelectric Double Perovskite Sr_2NiMoO_6 by Neutron Diffraction. *Mater. Res. Bull.* **2006**, *41*, 144−157.
(64) Ivanov, S. A.; Eriksson, S. G.; Tellgren, R.; Rundlöf, H.; Tseggai, M. The Magnetoelectric Perovskite Sr_2CoMoO_6: An Insight from Neutron Powder Diffraction. *Mater. Res. Bull.* **2005**, *40*, 840−849.
(65) Martínez-Lope, M. J.; Alonso, J. A.; Casais, M. T. Synthesis, Crystal and Magnetic Structure of the New Double Perovskite Ba_2MnMoO_6. *Z. Naturforsch. B* **2003**, *58*, 571−576.
(66) Cussen, E. J.; Vente, J. F.; Battle, P. D.; Gibb, T. C. Neutron Diffraction Study of the Influence of Structural Disorder on the Magnetic Properties of Sr_2FeMO_6 (M = Ta, Sb). *J. Mater. Chem.* **1997**, *7*, 459−463.
(67) Kashima, N.; Inoue, K.; Wada, T.; Yamaguchi, Y. Low Temperature Neutron Diffraction Studies of Sr_2FeMO_6 (M = Nb, Sb). *Appl. Phys. A* **2002**, *74*, s805−s807.
(68) Retuerto, M.; García-Hernández, M.; Martínez-Lope, M. J.; Fernández-Díaz, M. T.; Attfield, J. P.; Alonso, J. A. Switching from Ferro- to Antiferromagnetism in A_2CrSbO_6 (A = Ca, Sr) Double Perovskites: A Neutron Diffraction Study. *J. Mater. Chem.* **2007**, *17*, 3555−3561.
(69) Attfield, M. P.; Battle, P. D.; Bollen, S. K.; Gibb, T. C.; Whitehead, R. J. The Crystal Structure and Magnetic Properties of $SrLaFeSnO_6$ and $SrLaNiSbO_6$. *J. Solid State Chem.* **1992**, *100*, 37−48.
(70) Blanco, M. C.; Paz, S. A.; Nassif, V. M.; Guimpel, J. J.; Carbonio, R. E. Synthesis and Characterization of the New Two-Dimensional Heisenberg Antiferromagnet Double Perovskite $BaLaCuSbO_6$. *Dalton Trans.* **2015**, *44*, 10860−10866.

https://dx.doi.org/10.1021/acs.chemmater.0c02971
Chem. Mater. 2020, 32, 7070−7079